NEUROSCIENCE

A common hub for sleep and motor control in the substantia nigra

Danqian Liu[1], Weifu Li[2], Chenyan Ma[1], Weitong Zheng[1], Yuanyuan Yao[1], Chak Foon Tso[1], Peng Zhong[1], Xi Chen[2], Jun Ho Song[3], Woochul Choi[3], Se-Bum Paik[3], Hua Han[2], Yang Dan[1]*

The arousal state of the brain covaries with the motor state of the animal. How these state changes are coordinated remains unclear. We discovered that sleep–wake brain states and motor behaviors are coregulated by shared neurons in the substantia nigra pars reticulata (SNr). Analysis of mouse home-cage behavior identified four states with different levels of brain arousal and motor activity: locomotion, nonlocomotor movement, quiet wakefulness, and sleep; transitions occurred not randomly but primarily between neighboring states. The glutamic acid decarboxylase 2 but not the parvalbumin subset of SNr γ-aminobutyric acid (GABA)–releasing (GABAergic) neurons was preferentially active in states of low motor activity and arousal. Their activation or inactivation biased the direction of natural behavioral transitions and promoted or suppressed sleep, respectively. These GABAergic neurons integrate wide-ranging inputs and innervate multiple arousal-promoting and motor-control circuits through extensive collateral projections.

Many animals are immobile during sleep and in mammals diminished electromyographic (EMG) activity is a major criterion for identifying sleep (*1*–*4*). Although the correlation between brain state and motor activity is widely observed, the underlying mechanism remains poorly understood except for the dedicated circuit for rapid eye movement (REM) sleep atonia (*5*). One way to coordinate the changes is to use shared control circuits. γ-aminobutyric acid (GABA)–releasing (GABAergic) neurons in the substantia nigra pars reticulata (SNr) play a powerful role in movement suppression (*6*–*8*) and innervate multiple wake-promoting neuronal populations (*9*). Here, we investigated whether they participate in brain-state regulation.

First, we characterized the natural brain states and motor behaviors of the mice in their home cages on the basis of electroencephalographic (EEG), EMG, and video recordings (Fig. 1A). A deep learning algorithm was used for image segmentation and automated tracking of the mouse (Fig. 1B and fig. S1, A to E). Two parameters measuring body movement (translation and total movement) fell into three distinct clusters, corresponding to locomotion (LM), nonlocomotor movement (MV, including eating, grooming, and postural adjustments), and immobility. The immobility cluster was further divided into quiet wakefulness (QW) and sleep (SL, including REM and non-REM sleep) on the basis of EEG and EMG recordings (Fig. 1, C to E). These four states exhibit decreasing levels of motor activity and brain arousal, indicated by the decreasing EMG total power and increasing EEG delta power, respectively (Fig. 1F and fig. S1, F and G). Almost all transitions occurred between adjacent states; for example, direct transitions from LM to SL or from MV to SL were never observed (Fig. 1, G and H).

We next examined the activity of SNr neurons during these behavioral states. Recordings from freely moving mice in their home cages showed that some SNr neurons were preferentially active during states of high motor activity, exhibiting positive correlation coefficients (CCs) between their firing rates and EMG power (referred to as "movement-activated neurons"). Others exhibited the opposite profile ("movement-suppressed neurons"). Neurons with high baseline firing rates are more likely to be movement-activated neurons (fig. S2). Such functional diversity is consistent with previous findings (*10*, *11*), suggesting the existence of different cell types. Single-cell gene-expression analysis showed that parvalbumin (PV, encoded by *Pvalb*) and glutamic acid decarboxylase 2 (GAD2, encoded by *Gad2*) are preferentially expressed in separate SNr GABAergic populations (*12*). Indeed, in $Pvalb^{Cre}$ mice, Cre-inducible adeno-associated virus that expresses channelrhodopsin 2 fused with enhanced yellow fluorescent protein (AAV-DIO-ChR2-eYFP) labeled PV-positive neurons almost exclusively (96.1 ± 1.5% SEM), whereas in $Gad2^{Cre}$ mice it primarily labeled PV-negative neurons (92.3 ± 1.1%, referred to as "GAD2 neurons"; Fig. 2A and fig. S3, A and B). The two neuronal populations exhibited distinct spatial distributions, with PV neurons predominantly located in the lateral SNr and GAD2 neurons in the medial SNr (Fig. 2B). This allowed separate tagging of the two populations, which are thought to be involved in sensorimotor versus associative functions (*13*).

We then recorded from ChR2-tagged PV and GAD2 neurons. High-frequency laser pulses (15 and 30 Hz, 10 ms per pulse, 16 pulses per train) were applied intermittently, and single units exhibiting reliable laser-evoked spiking at short latencies were identified as PV or GAD2 neurons in the respective Cre mice (fig. S3, C to F). Many identified PV neurons showed high baseline firing rates and were most active during the LM or MV state (Fig. 2, C, G, and I). Of the 25 identified PV neurons, 22 were movement activated (CC between firing rate and EMG power > 0, $P < 0.05$) and only one was movement suppressed (fig. S3, G to I). Their mean firing rate showed a marked decrease at the MV→QW transition (termination of movement, $P = 0.026$, bootstrap) and an increase at the QW→MV transition (movement initiation, $P = 0.003$, Fig. 2E). By contrast, most of the GAD2 neurons identified in $Gad2^{Cre}$ mice showed low baseline firing rates; they were persistently active during SL and suppressed during periods of motor activity (Fig. 2, D, H, and I, and fig. S3, G to I). Their mean firing rate increased significantly at both movement termination (MV→QW transition, $P = 0.008$) and sleep initiation (QW→non-REM SL transition, $P = 0.018$) and decreased at sleep termination (SL→QW transition, $P = 0.003$, Fig. 2F).

We next tested the functions of GAD2 and PV neurons in regulating motor behaviors and brain states. Bilateral optogenetic activation of GAD2 neurons (2 min per trial applied randomly every 7 to 15 min) caused strong decreases in both LM and MV (Fig. 3, A and B, and movie S1). Compared with laser stimulation in control mice expressing eYFP only (fig. S4A), ChR2-mediated activation of GAD2 neurons significantly decreased movement initiation and increased movement termination ($P < 10^{-7}$, Kolmogorov–Smirnov test; Fig. 3D), consistent with the known function of SNr GABAergic neurons in movement suppression (*6*–*8*). Notably, GAD2 neuron activation also induced a rapid increase in SL ($P < 0.0001$, bootstrap; Fig. 3, A to C, and fig. S4, D and E), primarily by increasing the rate of sleep initiation (Fig. 3D). By contrast, although activation of SNr PV neurons also reduced MV ($P < 0.0001$), it had no effect on SL ($P = 0.81$; Fig. 3, A to C; fig. S4, G to I; and movie S2). Compared with control mice, the main effect of PV neuron activation was to increase movement termination through the MV→QW transition (Fig. 3, D and E).

We also tested the effects of inactivating SNr neurons through a light-activated chloride channel (iC++) (*14*). Inactivation of GAD2 neurons increased both LM and MV and greatly decreased SL (Fig. 3, F to I, and fig. S4, J to L),

[1]Division of Neurobiology, Department of Molecular and Cell Biology, Helen Wills Neuroscience Institute, Howard Hughes Medical Institute, University of California, Berkeley, CA 94720, USA. [2]National Laboratory of Pattern Recognition, Institute of Automation, Chinese Academy of Sciences, Beijing 100190, China. [3]Department of Bio and Brain Engineering, Korea Advanced Institute of Science and Technology, Daejeon 34141, Republic of Korea.
*Corresponding author. Email: ydan@berkeley.edu

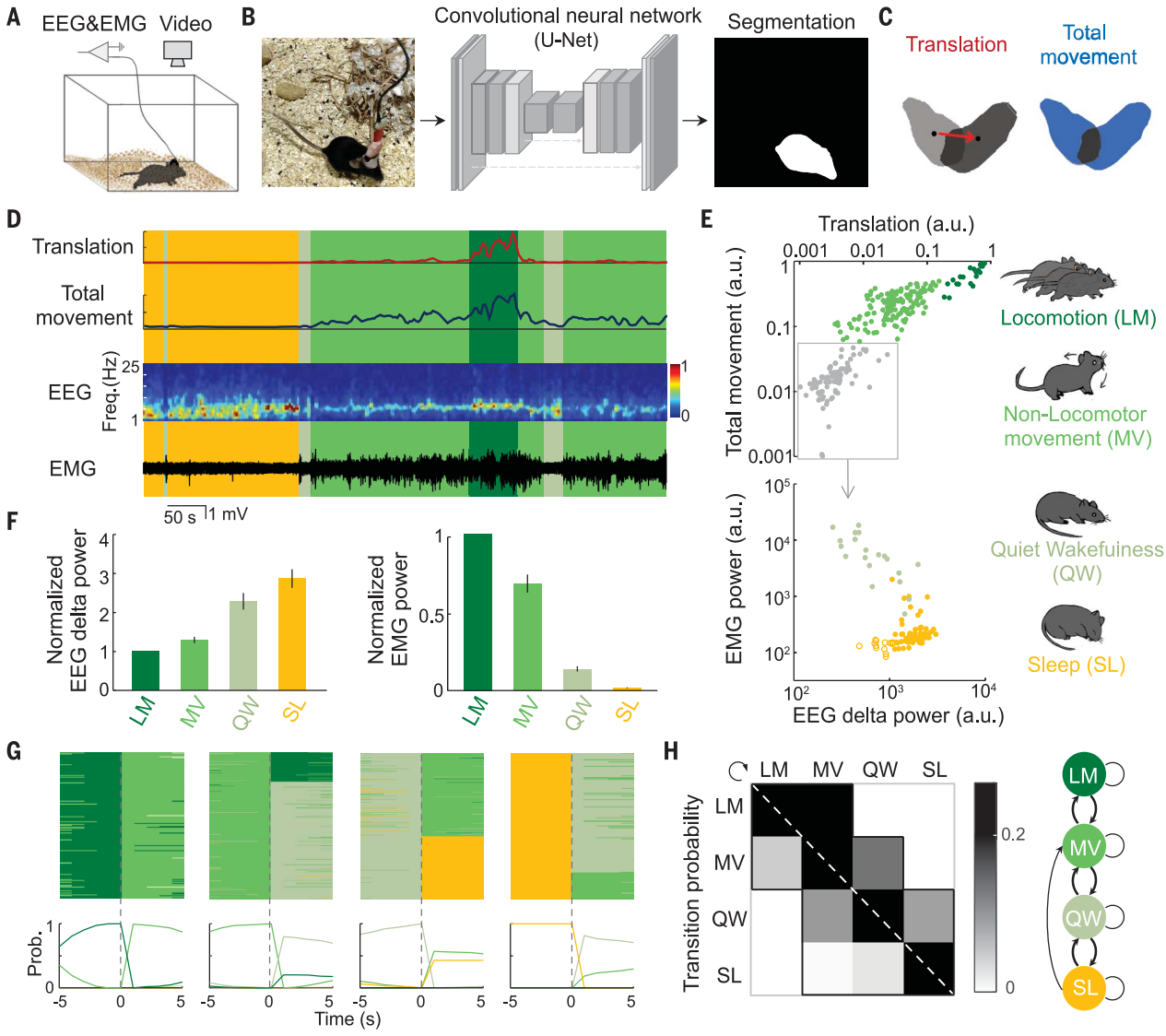

Fig. 1. Automated analysis of mouse home-cage behavior reveals nonrandom state transitions. (**A**) Schematic showing EEG, EMG, and video recordings of freely moving mice in their home cages. (**B**) Automated image segmentation. (**C**) Definition of translation (red arrow) and total movement (total area in blue). Black dots indicate the centroid of the segmented area. (**D**) Example recording showing translation, total movement, EEG spectrogram, and EMG trace. Freq., frequency. (**E**) Top, scatter plot for translation and total movement. Each dot represents data in a 2.5-s bin in (D). The three clusters correspond to LM, MV, and immobile states (gray box). Bottom, scatter plot for EEG delta power (1 to 4 Hz) and EMG total power during the immobile state. The two clusters correspond to QW and SL. Classified states are color-coded. Filled and open yellow, non-REM and REM sleep, respectively. a.u., arbitrary units. (**F**) Mean EEG delta power and EMG power during LM, MV, QW, and SL states (n = 9 mice). EEG delta and EMG power at different states were normalized by EEG delta and EMG power in the LM state, respectively. Error bar indicates ± SEM. (**G**) Top, all transitions from each state. T = 0, time of transition. Bottom, probability (Prob.) of each state before and after transition. (**H**) Left, probability of transition between each pair of states. Right, summary of all natural transitions.

indicating the importance of their endogenous spiking activity in movement suppression and sleep generation. Inactivation of PV neurons also reduced SL, but the effect was much weaker than that of GAD2 neuron inactivation (Fig. 3, F to H, and fig. S4, M to O); a main effect of PV neuron inactivation was to decrease movement termination (Fig. 3, I and J). The different contributions of GAD2 and PV neurons to sleep generation were further confirmed by the effects of chemogenetic activation and inactivation of each population (fig. S5).

Although optogenetic activation of GAD2 neurons caused strong enhancement of movement termination and sleep initiation (Fig. 3D), we observed no direct LM→SL or MV→SL transitions, which were absent in normal home-cage behavior (Fig. 1, G and H). Instead, laser stimulation significantly increased the naturally occurring LM→MV, MV→QW, and QW→SL transitions, all in the direction of decreasing arousal and motor activity; transitions in the opposite direction were strongly suppressed (Fig. 3E). GAD2 neuron activation also increased nest entering, and SL during the activation occurred almost exclusively within the nest, similar to SL without laser stimulation (fig. S4, B and C). Optogenetic inactivation of SNr GAD2 neurons also induced no artificial transition and its effects were caused entirely by enhancing or suppressing the natural transitions in the direction of increasing or decreasing motor activity and EEG activation, respectively (Fig. 3J).

Anterograde tracing of SNr neuron axons expressing ChR2-eYFP showed that PV neurons

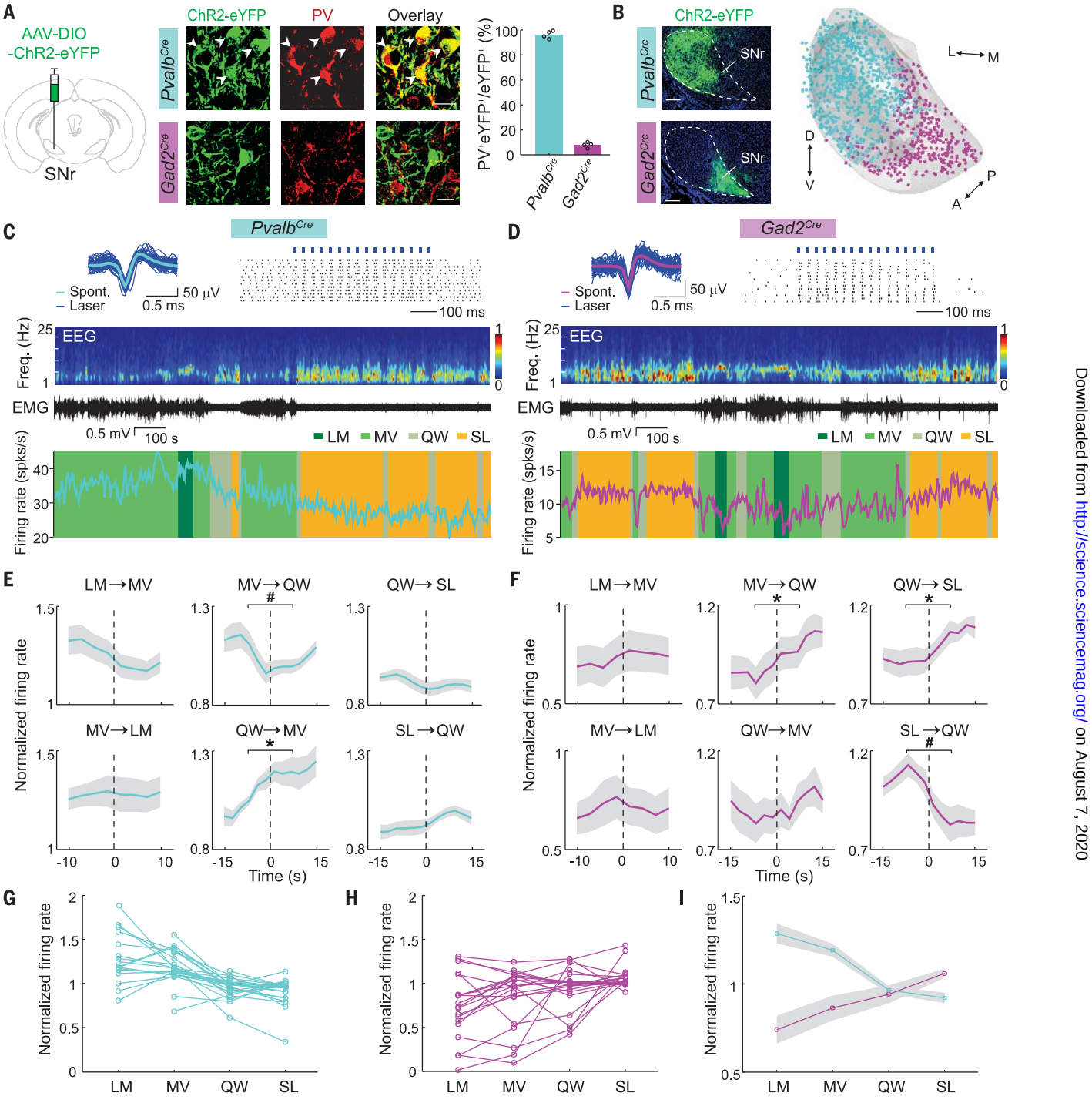

Fig. 2. PV and GAD2 neurons in the SNr show distinct behavioral state–dependent firing rates. (**A**) Left, immunostaining of eYFP and PV in *Pvalb*^{Cre} (top) and *Gad2*^{Cre} (bottom) mice injected with AAV-DIO-ChR2-eYFP. Arrowheads indicate colabeled neurons. Scale bar, 20 μm. Right, percentages of eYFP-labeled neurons that are PV positive (n = 4 mice). (**B**) Fluorescence images (left) and three-dimensional reconstruction (right) of eYFP-labeled PV and GAD2 SNr neurons. Scale bar, 200 μm. (**C**) Example recording from an identified PV neuron. Top left, laser-evoked and spontaneous (Spont.) spike waveforms. Top right, spike raster. Blue ticks, laser pulses (30 Hz). Bottom, firing rate of the PV neuron together with EEG spectrogram, EMG trace, and behavioral states. spks, spikes. (**D**) Similar to (C) but for an identified GAD2 neuron. (**E**) Normalized mean firing rate of all identified PV neurons at behavioral state transitions (n = 25). Vertical line, transition point. Shading indicates ±SEM. *Significant increase at $P < 0.05$, bootstrap. #Significant decrease at $P < 0.05$, bootstrap. (**F**) Similar to (E) but for GAD2 neurons (n = 22). (**G** and **H**) Normalized firing rate for individual neurons during different states. Each line indicates one neuron. For some neurons, no LM was detected during recording. (**I**) Firing rate averaged across all identified PV or GAD2 neurons. Shading indicates ±SEM.

project primarily to brain regions involved in movement control, such as the motor thalamus, motor layers of the superior colliculus (SCm), and the mesencephalic locomotor region (MLR), including the midbrain reticular nucleus (MRN) and the pedunculopontine nucleus (PPN) (*15*) (Fig. 4, A to C; table S1, and movie S3). By contrast, GAD2 neurons also project to several regions involved in brain-state regulation. These include monoaminergic centers such as the dorsal raphe nucleus (DR), locus ceruleus (LC), and ventral tegmental area (VTA; fig. S6, A and B), where SNr neurons directly innervate serotonergic, noradrenergic, and dopaminergic neurons (*9*, *16*, *17*). The

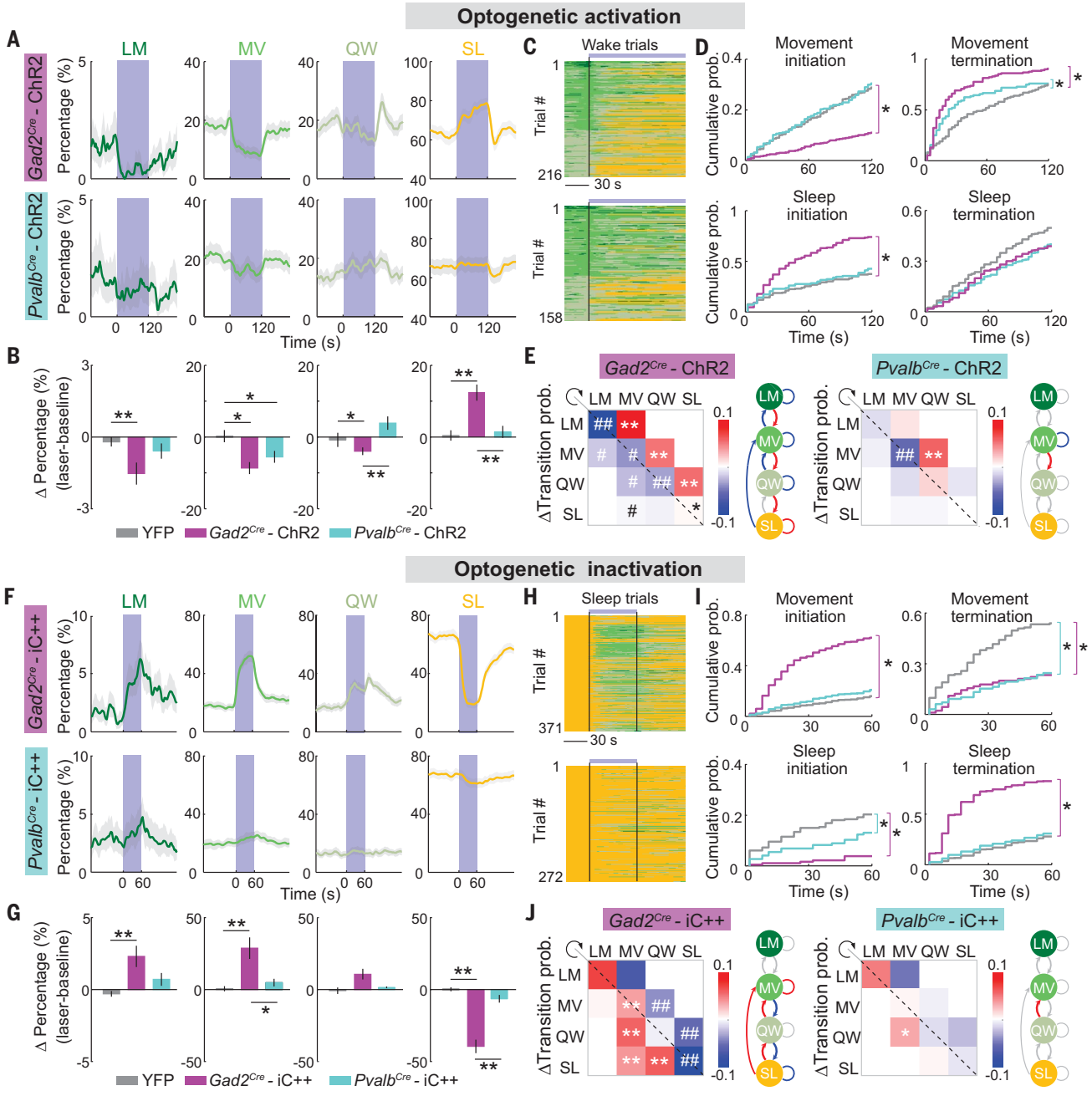

Fig. 3. Causal effects of SNr GAD2 and PV neuron activity on motor behavior and sleep. (**A**) Percentage of time in LM, MV, QW, or SL state before, during, and after laser activation of SNr neurons in *Gad2*^{Cre}-ChR2 mice (top, n = 7 mice, P_{LM}, P_{MV}, P_{QW}, P_{SL} < 0.0001, bootstrap) or *Pvalb*^{Cre}-ChR2 mice (bottom, n = 7, P_{LM} = 0.051, P_{MV} < 0.0001, P_{QW} = 0.0009, P_{SL} = 0.81). Shading indicates 95% confidence intervals. Blue stripe indicates the laser period (constant light, 120 s). (**B**) Laser-induced changes in each state in *Gad2*^{Cre}-ChR2, *Pvalb*^{Cre}-ChR2, or eYFP control mice (n = 6). Error bars indicate SEM. *P < 0.05, **P < 0.01, Mann–Whitney U test. (**C**) Behavioral states in all "wake trials" (mice stayed awake for >30 s before laser onset). (**D**) Cumulative probabilities for movement initiation or termination and sleep initiation or termination during 120-s laser stimulation. *$P < 10^{-7}$ for comparison between ChR2 and eYFP control experiments, Kolmogorov–Smirnov test. (**E**) Laser-induced changes in transition probability. *Increase, P < 0.05, bootstrap. #Decrease, P < 0.05, bootstrap. **Increase, P < 0.0005. ##Decrease, P < 0.0005. (**F**) Similar to (A) but for iC++-mediated inactivation (constant light, 60 s) in *Gad2*^{Cre} mice (top, n = 6, P_{LM}, P_{MV}, P_{QW}, P_{SL} < 0.0001) or *Pvalb*^{Cre} mice (bottom, n = 5, P_{LM} = 0.88, P_{MV} = 0.0034, P_{QW} = 0.88, P_{SL} = 0.0002). (**G**) Similar to (B) but for optogenetic inactivation. (**H**) Similar to (C) but for all sleep trials in inactivation experiments. (**I** and **J**) Similar to (D) and (E) but for optogenetic inactivation.

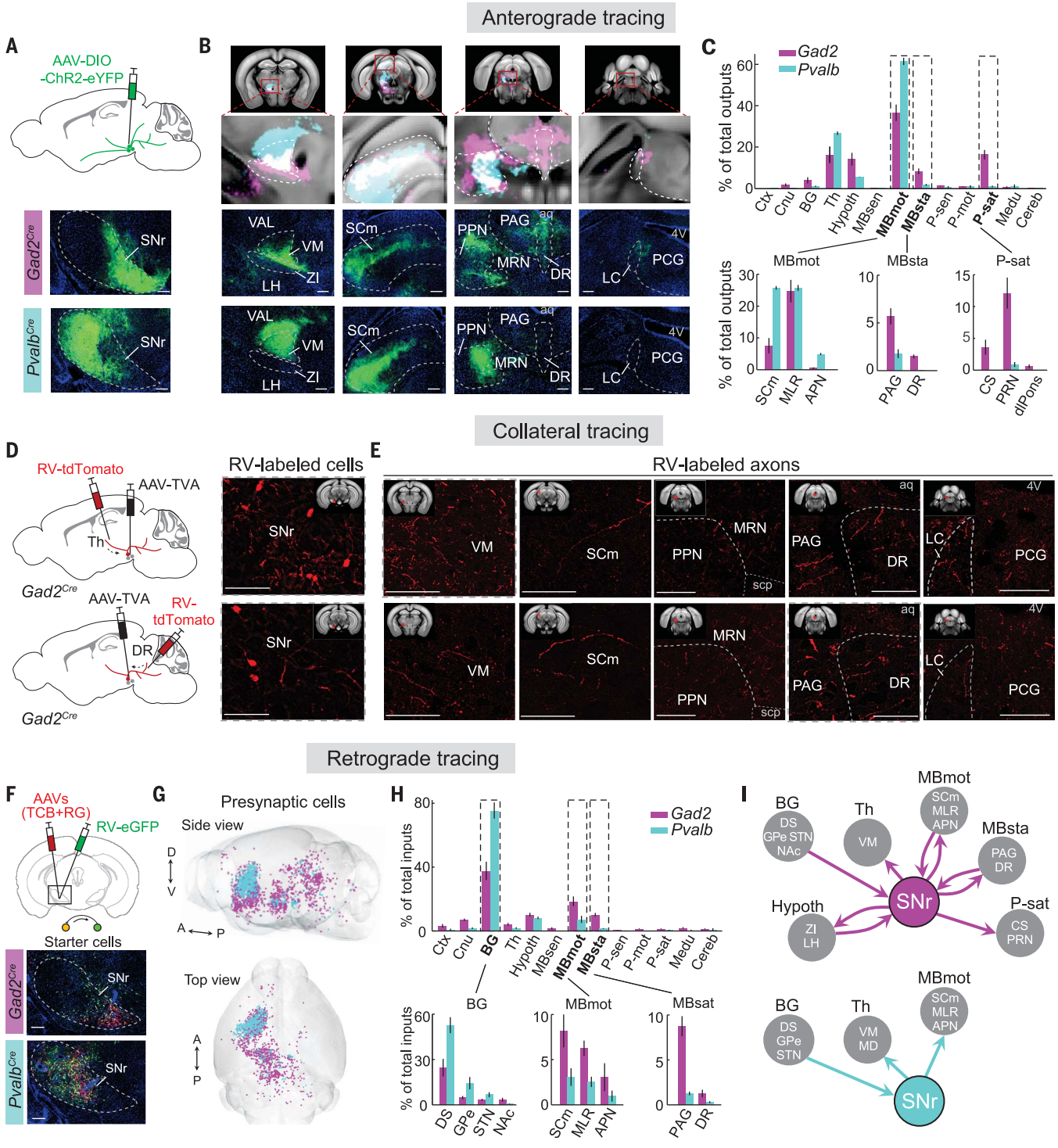

Fig. 4. Whole-brain mapping of outputs and inputs of SNr GAD2 and PV neurons. (**A**) Fluorescence images showing ChR2-eYFP expression in *Gad2*^{Cre} or *Pvalb*^{Cre} mouse SNr. (**B**) Summary (top) and example images showing labeled axons. VM, ventral medial complex of the thalamus; VAL, ventral anterior-lateral complex of the thalamus; ZI, zona incerta; LH, lateral hypothalamic area; PAG, periaqueductal gray; PCG, pontine central gray; aq, cerebral aqueduct; 4V, fourth ventricle. Scale bars, 200 μm for (A) and (B). (**C**) Percentages of labeled axons in 13 main brain regions (top, n = 3 mice each) and specific structures (bottom). The MLR includes the MRN and PPN. Abbreviations are defined in table S1. (**D**) Fluorescence images of RV-labeled SNr GAD2 neurons projecting to the thalamus (top) or DR (bottom). (**E**) Axonal collaterals in multiple regions. Scp, superior cerebellar peduncles. Scale bars, 100 μm for (D) and (E). (**F**) Monosynaptic retrograde tracing from GAD2 and PV neurons. Fluorescence images show starter cells (yellow) in the SNr. Scale bars, 200 μm. (**G**) Whole-brain reconstruction of inputs to SNr neurons in a *Gad2*^{Cre} mouse (magenta, n = 1200 input cells) or a *Pvalb*^{Cre} mouse (cyan, n = 1088). Injection site is excluded. (**H**) Similar to (C) but for input distribution for GAD2 (n = 5 mice) and PV neurons (n = 5). (**I**) Diagram summarizing major connections for SNr GAD2 and PV neurons.

projections of SNr GAD2 neurons are also different from those of VTA GABAergic neurons, which powerfully promote non-REM sleep but rarely innervate motor thalamus or MLR (*18*, *19*).

The divergent projections of GAD2 neurons could either originate from different SNr subpopulations or represent axon collaterals of the same neurons. To label the axon collaterals of thalamus-projecting GAD2 neurons, we injected a Cre-inducible AAV that expresses avian-specific retroviral receptor, TVA, into the SNr of *Gad2*^{Cre} mice. A modified rabies virus (RV) expressing tdTomato (RV-ΔG-tdTomato+EnvA) was injected 2 weeks later into the thalamus, which allowed RV to enter the TVA-expressing axons, be transported retrogradely to the SNr neurons, and label all of their axon collaterals with tdTomato (Fig. 4D). In addition to the thalamus, we found labeled axons in the SCm, MRN and PPN, DR, LC, and VTA (Fig. 4E and fig. S6, C and D). Similarly, injection of the RV into the DR revealed labeled axons in the thalamus, SCm, MRN and PPN, LC, and VTA. Each SNr GAD2 neuron thus sends axon collaterals to multiple brain regions differentially involved in motor and brain-state control (fig. S7).

Finally, we used RV-mediated transsynaptic tracing to identify monosynaptic inputs to SNr PV and GAD2 neurons. AAVs expressing rabies glycoprotein and TVA fused with mCherry (TCB) were injected into the SNr of each Cre mouse, followed by injection of a modified RV expressing eGFP (RV-ΔG-eGFP+EnvA) 2 weeks later (Fig. 4F). In *Pvalb*^{Cre} mice, the vast majority (75.5 ± 5.0%) of eGFP-labeled input neurons were found within the basal ganglia (Fig. 4, G and H; fig. S8; table S1; and movie S4). By contrast, inputs to GAD2 neurons were much more distributed, with substantial fractions in the hypothalamus and midbrain regions. Thus, whereas PV neurons serve mainly as a basal ganglia output to motor-control regions, GAD2 neurons integrate a much wider range of inputs and project broadly to brain-state as well as motor-control regions (Fig. 4I).

We found that GAD2 but not PV neuron activity promotes sleep generation (primarily non-REM sleep initiation). PV neurons in the lateral SNr fire at higher rates in states of high motor activity and their activation or inactivation increased or decreased movement termination, consistent with a proposed function of the SNr in suppressing unwanted movements during action selection (*20*). By contrast, GAD2 neurons in the medial SNr were preferentially active in states of low motor activity. In addition to motor suppression, their activation powerfully enhanced the transition from QW to SL. This indicates that SNr GAD2 neurons provide general suppression of both motor activity and brain arousal to promote states of quiescence. The involvement of some SNr neurons in sleep regulation is consistent with previous lesion studies in rats (*21*, *22*) and cats (*23*). Within the basal ganglia, activation of adenosine A2A receptor–expressing GABAergic neurons in the striatum or neurotensin-expressing glutamatergic neurons in the subthalamic nucleus also increased sleep (*24*, *25*) (fig. S9). Because these neurons are all part of the basal ganglia indirect pathway (*8*), their sleep-promoting effects are likely mediated, at least in part, by activation of the SNr GAD2 neurons.

Activation of SNr GAD2 neurons suppressed movement and enhanced sleep by biasing the direction of natural state transitions rather than by causing abrupt cessation of all motor activity (behavioral arrest). The LM→MV→QW→SL behavioral sequence promoted by GAD2 neuron activation was characterized by a progressive decrease in motor activity and increase in EEG delta power. Coordination of behavioral and brain-state changes could be mediated by multiple cell types. For example, LC noradrenergic neurons regulate motor activity as well as brain arousal (*26*), and PPN neurons control both locomotion and cortical activation (*15*, *27*–*30*). By innervating these populations through extensive collateral projections while integrating inputs from wide-ranging brain areas, the SNr GAD2 neurons serve as a critical hub in a common circuit for sleep and motor control.

REFERENCES AND NOTES

1. S. S. Campbell, I. Tobler, *Neurosci. Biobehav. Rev.* **8**, 269–300 (1984).
2. J. C. Hendricks *et al.*, *Neuron* **25**, 129–138 (2000).
3. P. J. Shaw, C. Cirelli, R. J. Greenspan, G. Tononi, *Science* **287**, 1834–1837 (2000).
4. D. Liu, Y. Dan, *Annu. Rev. Neurosci.* **42**, 27–46 (2019).
5. J. Peever, P. M. Fuller, *Curr. Biol.* **27**, R1237–R1248 (2017).
6. O. Hikosaka, R. H. Wurtz, *J. Neurophysiol.* **53**, 292–308 (1985).
7. A. V. Kravitz *et al.*, *Nature* **466**, 622–626 (2010).
8. C. R. Gerfen, D. J. Surmeier, *Annu. Rev. Neurosci.* **34**, 441–466 (2011).
9. C. Ma *et al.*, *Neuron* **103**, 323–334.e7 (2019).
10. X. Jin, F. Tecuapetla, R. M. Costa, *Nat. Neurosci.* **17**, 423–430 (2014).
11. G. Rizzi, K. R. Tan, *Cell Rep.* **27**, 2184–2198.e4 (2019).
12. A. Saunders *et al.*, *Cell* **174**, 1015–1030.e16 (2018).
13. N. Rajakumar, K. Elisevich, B. A. Flumerfelt, *J. Comp. Neurol.* **350**, 324–336 (1994).
14. A. Berndt *et al.*, *Proc. Natl. Acad. Sci. U.S.A.* **113**, 822–829 (2016).
15. T. K. Roseberry *et al.*, *Cell* **164**, 526–537 (2016).
16. S. K. Ogawa, J. Y. Cohen, D. Hwang, N. Uchida, M. Watabe-Uchida, *Cell Rep.* **8**, 1105–1118 (2014).
17. B. Weissbourd *et al.*, *Neuron* **83**, 645–662 (2014).
18. X. Yu *et al.*, *Nat. Neurosci.* **22**, 106–119 (2019).
19. S. Chowdhury *et al.*, *eLife* **8**, e44928 (2019).
20. G. Cui *et al.*, *Nature* **494**, 238–242 (2013).
21. D. Gerashchenko, C. A. Blanco-Centurion, J. D. Miller, P. J. Shiromani, *Neuroscience* **137**, 29–36 (2006).
22. M. H. Qiu, R. Vetrivelan, P. M. Fuller, J. Lu, *Eur. J. Neurosci.* **31**, 499–507 (2010).
23. Y. Y. Lai *et al.*, *Neuroscience* **90**, 469–483 (1999).
24. Y. Oishi *et al.*, *Nat. Commun.* **8**, 734 (2017).
25. X. S. Yuan *et al.*, *eLife* **6**, e29055 (2017).
26. J. C. Holstege, H. G. Kuypers, *Neuroscience* **23**, 809–821 (1987).
27. A. M. Lee *et al.*, *Neuron* **83**, 455–466 (2014).
28. V. Caggiano *et al.*, *Nature* **553**, 455–460 (2018).
29. D. Kroeger *et al.*, *J. Neurosci.* **37**, 1352–1366 (2017).
30. D. J. Galtieri, C. M. Estep, D. L. Wokosin, S. Traynelis, D. J. Surmeier, *eLife* **6**, e30352 (2017).

ACKNOWLEDGMENTS

We thank F. Weber and M. Xu for data analysis, Q. Xie and H. Ren for deep learning analysis, Y. Zuo and S. Ma for collateral tracing, W. Chang for rabies virus, and J. Ding for helpful comments. **Funding:** This work was supported by the Howard Hughes Medical Institute. **Author contributions:** D.L. and Y.D. designed the experiments and wrote the manuscript; D.L. performed most experiments and data analysis; W.L., X.C., and H.H. performed deep learning analysis; J.H.S., W.C., and S.-B.P. developed the AMaSiNe software; W.Z., C.M., Y.Y., C.F.T., and P.Z. performed histology and FISH experiments; and Y.D. supervised all aspects of the project. **Competing interests:** The authors declare no competing interests. **Data and materials availability:** All data necessary to understand and assess the conclusions of this study are available in the manuscript or the supplementary materials. The viruses used in this work were provided under a materials transfer agreement with Stanford University.

SUPPLEMENTARY MATERIALS

science.sciencemag.org/content/367/6476/440/suppl/DC1
Materials and Methods
Figs. S1 to S9
Table S1
Captions for Movies S1 to S4
References (*31*–*39*)

View/request a protocol for this paper from *Bio-protocol*.

13 August 2019; accepted 29 November 2019
10.1126/science.aaz0956

Science

A common hub for sleep and motor control in the substantia nigra

Danqian Liu, Weifu Li, Chenyan Ma, Weitong Zheng, Yuanyuan Yao, Chak Foon Tso, Peng Zhong, Xi Chen, Jun Ho Song, Woochul Choi, Se-Bum Paik, Hua Han and Yang Dan

Science **367** (6476), 440-445.
DOI: 10.1126/science.aaz0956

Interneurons control brain arousal states

The underlying circuit mechanisms coordinating brain arousal and motor activity are poorly understood. Liu *et al.* found that glutamic acid decarboxylase 2 (GAD2)–expressing, but not parvalbumin-expressing, interneurons in a part of the brain known as the substantia nigra promote sleep (see the Perspective by Wisden and Franks). Parvalbuminergic neurons fire at higher rates in states of high motor activity, and their activation increases movement termination consistent with the function of the substantia nigra in suppressing unwanted movements during action selection. By contrast, GAD2 neurons are preferentially active in states of low motor activity. In addition to motor suppression, their activation powerfully enhances the transition from quiet wakefulness to sleep, which differ mainly in the arousal level rather than motor behavior. GAD2 interneurons thus provide general suppression of both motor activity and brain arousal to promote states of quiescence.

Science, this issue p. 440; see also p. 366

Science (print ISSN 0036-8075; online ISSN 1095-9203) is published by the American Association for the Advancement of Science, 1200 New York Avenue NW, Washington, DC 20005. The title *Science* is a registered trademark of AAAS.